Comprehensive Control of Matrix Converters in On-Board Electric Drive Applications

Galina Mirzaeva
THE UNIVERSITY OF NEWCASTLE
University Drive
Callaghan, NSW2308, Australia
Phone: +61 (2) 4921-6083
Fax: +61 (2) 4921-6993
Email: Galina.Mirzaeva@newcastle.edu.au

Acknowledgments

This research was partially supported by the Australian Government through the Australian Research Council's Discovery Projects funding scheme (project DP2201039287).

Keywords

≪AC-AC Converter≫, ≪Matrix Converter≫, ≪Converter control≫, ≪Power converters for EV≫, ≪State and disturbance observers≫.

Abstract

Matrix Converters are an attractive alternative to the traditional AC/DC/AC converters, particularly, in electric transportation. Their advantages include low weight and volume, high reliability and efficiency. However, variable frequency and variable power operation, typical for electric vehicles, poses control challenges. This paper addresses these challenges and proposes a robust control solution for Matrix Converters with a number of novel features. The paper compares the proposed and the conventional control schemes for Matrix Converters, and shows improvement with respect to power factor control, input resonance suppression, reference tracking and harmonics performance. Findings of the paper are supported by simulations results.

Introduction

A Direct Matrix Converter (DMC) is illustrated in in Fig.1a. Unlike the conventional two-stage AC/ DC/AC conversion option, Matrix Converter (MC) does not require an intermediate DC-link energy storage. This leads to a more compact, power efficient and reliable design [1]. Only a small RLC filter is needed on the MC input side, to prevent harmonic pollution of the supply.

Over the past decade, the MC technology has seen many applications including AC drives, power quality compensators, renewable energy integration and grid interface [2]. Currently, MC are being introduced to electric vehicles [3]. This has posed new challenges to the MC control. A larger number of control objectives need to be satisfied simultaneously, while the available degrees of freedom in MC are very limited. As with any electric drive application, the load side objectives include accurate reference tracking and low harmonic distortion. Additionally, at the input side, active damping of the input filter resonance, low harmonic distortion and power factor correction at the supply are desired.

Conventional MC control schemes include closed-loop control of the output (load) side current and have similarities to Field Oriented Control (FOC) used with standard AC drives [4]. The control action, in the form of a switched output voltage vector $\bar{v}_o = v_o \angle \alpha_o$, is typically implemented by Space Vector

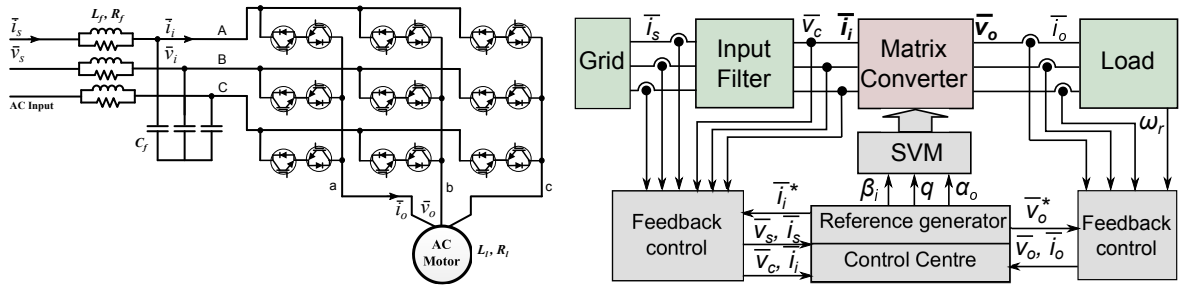

(a) Direct Matrix Converter (b) Comprehensive MC control scheme

Fig. 1: Direct Matrix Converter and the proposed Comprehensive control.

Modulation (SVM). SVM for MC, discussed in detail in [5], has room for additional control of the angle β_i of the input current vector ($\bar{i}_i = i_i \angle \beta_i$). This is typically utilised to achieve unity power factor at the supply side [6]. If active damping of the input filter resonance is also desired, some form of trade-off between the input and the output control is applied.

For example, control of the MC output current can be performed indirectly, by closed-loop control of the MC input current [7]. This approach allows for including extra loops for power factor control and active damping. An alternative, MPC, approach is explored in [8, 9]. It provides indirect active damping by penalising the input current error together with the load current error in a cost function. To achieve harmonic performance comparable to SVM, modulated MPC can be used [10].

The authors of the current paper propose a new Comprehensive control method, called so because it seamlessly matches the competing control objectives on both MC sides. The Comprehensive control scheme is illustrated in Fig.1b. Standard measurements performed at the supply and load sides of MC are used by "Reference generator" to produce references that are compatible with each other. State feedback control is then used to regulate both the load- and the supply-side current around the corresponding references. The use of observers guarantees zero steady-state errors at both sides.

The proposed control scheme provides excellent tracking performance of the load-side current, as well as unity power factor, active damping and harmonic suppression at the supply side. These features, combined with weight and volume advantages of an MC, make it a very attractive solution for on-board drives in air, sea or road electric transportation. This paper compares the proposed control scheme with the conventional MC control, with respect to the above performance indicators. It demonstrates, by simulation, the advantages of the proposed scheme.

Comprehensive control for Matrix Converter

Supply side model

An RLC filter (with parameters R_f, L_f, C_f) typically connects the supply with the input side of the MC. The associated voltages and currents in each phase $\phi \in \{\alpha, \beta\}$, can be modelled in continuous time by the following second order dynamic system:

$$\frac{\mathrm{d}(\mathbf{x}_i^\phi)}{\mathrm{d}t} = \mathbf{A}_i \mathbf{x}_i^\phi + \mathbf{B}_i \begin{bmatrix} v_s^\phi \\ i_i^\phi \end{bmatrix}; \quad \mathbf{x}_i^\phi \doteq \begin{bmatrix} i_s^\phi \\ v_i^\phi \end{bmatrix}; \quad \mathbf{A}_i = \begin{bmatrix} -\frac{R_f}{L_f} & -\frac{1}{L_f} \\ \frac{1}{C_f} & 0 \end{bmatrix}; \quad \mathbf{B}_i = \begin{bmatrix} \frac{1}{L_f} & 0 \\ 0 & -\frac{1}{C_f} \end{bmatrix} \tag{1}$$

where v_s^ϕ and i_s^ϕ are the supply voltage and current in phase $\phi \in \{\alpha, \beta\}$, and v_i^ϕ, i_i^ϕ are the voltage and current at the input of the MC in the same phase.

According to the Internal Model Principle [11], rejection of a disturbance requires its inclusion in the

system model. Hence it is proposed to include in the supply side model a disturbance model of the form:

$$\frac{\mathrm{d}(\mathbf{x}_i^{\phi})}{\mathrm{d}t} = \mathbf{A}_i\mathbf{x}_i^{\phi} + \mathbf{B}_i\begin{bmatrix} v_s^{\phi} \\ i_i^{\phi} \end{bmatrix} + \begin{bmatrix} d_1^{\phi} \\ d_2^{\phi} \end{bmatrix};\ \frac{\mathrm{d}(\mathbf{d}_i)}{\mathrm{d}t} = \mathbf{A}_{di}\mathbf{d}_i;\ \mathbf{d}_i \doteq \begin{bmatrix} d_1^{\alpha} \\ d_1^{\beta} \\ d_2^{\alpha} \\ d_2^{\beta} \end{bmatrix};\ \mathbf{A}_{di} = \begin{bmatrix} 0 & -\omega_i & 0 & 0 \\ \omega_i & 0 & 0 & 0 \\ 0 & 0 & 0 & -\omega_i \\ 0 & 0 & \omega_i & 0 \end{bmatrix} \quad (2)$$

where $d_1^{\alpha,\beta}$ and $d_2^{\alpha,\beta}$ are harmonic disturbances, at the supply frequency ω_i, for $i_s^{\alpha,\beta}$ and $v_c^{\alpha,\beta}$, respectively.

Load side model

The load side model corresponds to an RL load with parameters R_l, L_l. Similarly to the supply side, it is proposed to include a disturbance at ω_o in the load side model as:

$$\frac{\mathrm{d}(i_o^{\phi})}{\mathrm{d}t} = -a_o i_o^{\phi} + b_o v_o^{\phi} + d_o^{\phi};\quad \frac{\mathrm{d}(\mathbf{d}_o)}{\mathrm{d}t} = \mathbf{A}_{do}\mathbf{d}_o;\qquad \mathbf{d}_o \doteq \begin{bmatrix} d_o^{\alpha} \\ d_o^{\beta} \end{bmatrix};\quad \mathbf{A}_{do} = \begin{bmatrix} 0 & -\omega_o \\ \omega_o & 0 \end{bmatrix} \quad (3)$$

where v_o^{ϕ}, i_o^{ϕ} are the load voltage and current in one of the output phases $\phi \in \{\alpha, \beta\}$; $a_o = R_l/L_l$; $b_o = 1/L_l$; and d_o^{ϕ} is harmonic disturbance, at the load side frequency ω_o, for i_o^{ϕ} in the same phase.

For the control computation, discrete-time state-space equivalents of (2) and (3) are used.

Input and output side observers

To achieve integral action at the desired fundamental frequencies, it is suggested to complement the extended models (2) and (3) by the observers, for all state and disturbances variables, as follows.

$$\frac{\mathrm{d}(\hat{\mathbf{x}}_i^{\phi})}{\mathrm{d}t} = \mathbf{A}_i\hat{\mathbf{x}}_i^{\phi} + \mathbf{B}_i\begin{bmatrix} v_s^{\phi} \\ i_i^{\phi} \end{bmatrix} + \begin{bmatrix} \hat{d}_1^{\phi} \\ \hat{d}_2^{\phi} \end{bmatrix} + \mathbf{J}_i(\mathbf{x}_i^{\phi} - \hat{\mathbf{x}}_i^{\phi});\qquad \frac{\mathrm{d}(\hat{\mathbf{d}}_i)}{\mathrm{d}t} = \mathbf{A}_{di}\hat{\mathbf{d}}_i + \mathbf{J}_{di}(\mathbf{x}_i^{\phi} - \hat{\mathbf{x}}_i^{\phi}); \quad (4)$$

$$\frac{\mathrm{d}(\hat{i}_o^{\phi})}{\mathrm{d}t} = a_o\hat{i}_o^{\phi} + b_o v_o^{\phi} + \hat{d}_o^{\phi} + \mathbf{J}_o(i_o^{\phi} - \hat{i}_o^{\phi});\qquad \frac{\mathrm{d}(\hat{\mathbf{d}}_o)}{\mathrm{d}t} = \mathbf{A}_{do}\hat{\mathbf{d}}_o + \mathbf{J}_{do}(i_o^{\phi} - \hat{i}_o^{\phi}). \quad (5)$$

where $\mathbf{J}_i$, $\mathbf{J}_o$, $\mathbf{J}_{di}$ and $\mathbf{J}_{do}$ are matrices of observers gains of appropriate dimensions.

Introduction of the observers has the following important effect. Irrespective of the model accuracy, if a steady state trajectory is reached, then $\hat{\mathbf{x}}_i \to \mathbf{x}_i$, $\hat{i}_o \to i_o$, at the respective disturbance frequencies. In other words, the system models may include parameter errors and unmodelled terms, such as, for instance, a missing back-emf in (3) or incorrectly defined supply voltage in (1). Regardless of that, due to the inclusion of the disturbance models in (2) and (3), "integral action" is provided by observers (4) and (5), and the estimated system states ($\hat{i}_s$, $\hat{v}_i$, $\hat{i}_o$) will have zero errors at frequencies ω_i and ω_o, respectively.

Steady state input and output side references

The load and the supply sides are required to track sinusoidal steady state references, and quickly transition to a new steady state if the load conditions change. In Fig.1b the sinusoidal steady state references (i_s^*, v_i^* and i_o^*) and the corresponding steady state MC signals (i_i^*, v_o^*) are calculated by "Reference generator" as follows. When in steady state, the MC supply side and load side models satisfy the trajectories obtained by using standard circuit theory. Additionally, the supply and the load side references and MC signals are linked by two steady state conditions, namely, real power balance across the switches and the desired (e.g. unity) power factor at the supply. This yields the following eight steady state equations:

$$Input\begin{cases} -L_f\omega_i i_s^{*\beta} + R_f i_s^{*\alpha} = v_s^{*\alpha} - v_i^{*\alpha} + L_f\hat{d}_1^{\alpha} \\ L_f\omega_i i_s^{*\alpha} + R_f i_s^{*\beta} = v_s^{*\beta} - v_i^{*\beta} + L_f\hat{d}_1^{\beta} \\ -C_f\omega_i v_i^{*\beta} = i_s^{*\alpha} - i_i^{*\alpha} + C_f\hat{d}_2^{\alpha} \\ C_f\omega_i v_i^{*\alpha} = i_s^{*\beta} - i_i^{*\beta} + C_f\hat{d}_2^{\beta} \end{cases} \qquad Output\begin{cases} -L_l\omega_o i_o^{*\beta} + R_l i_o^{*\alpha} = v_o^{*\alpha} + L_l\hat{d}_o^{\alpha} \\ L_l\omega_o i_o^{*\alpha} + R_l i_o^{*\beta} = v_o^{*\beta} + L_l\hat{d}_o^{\beta} \end{cases}$$

$$Extra\begin{cases} v_i^{*\alpha} i_i^{*\alpha} + v_i^{*\beta} i_i^{*\beta} = v_o^{*\alpha} i_o^{*\alpha} + v_o^{*\beta} i_o^{*\beta} \\ v_s^{*\alpha} i_s^{*\beta} - v_s^{*\beta} i_s^{*\alpha} = 0 \end{cases} \quad (6)$$

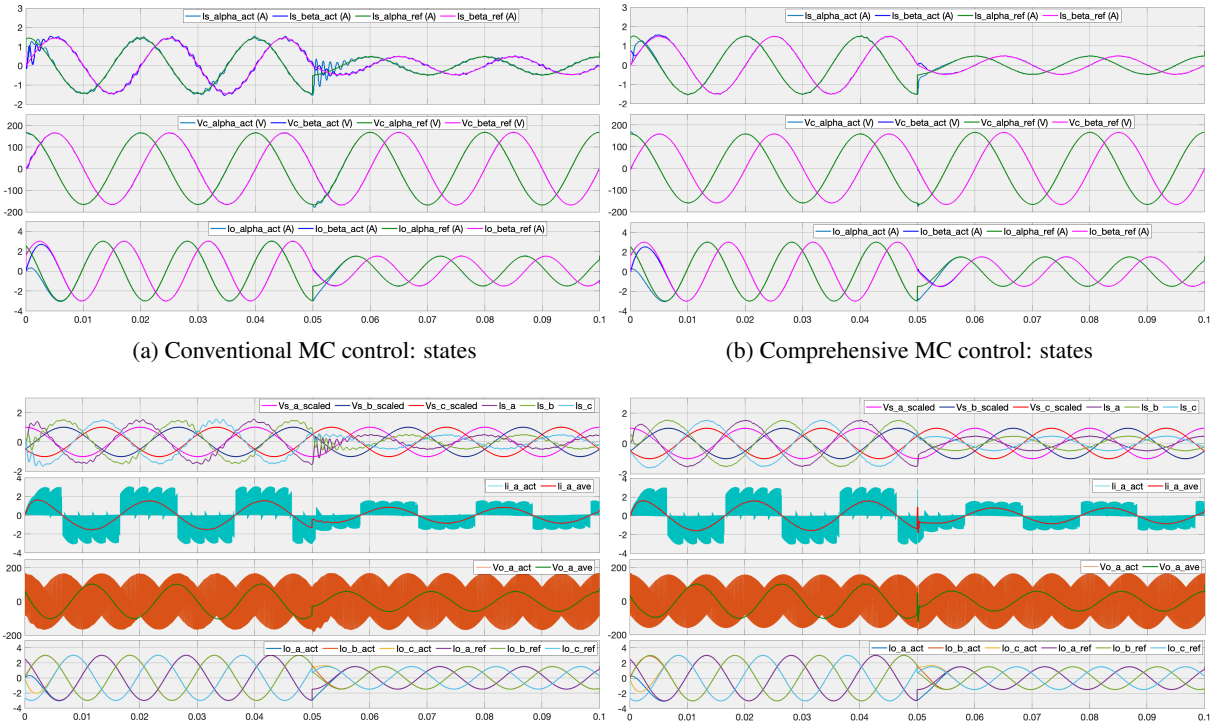

(a) Conventional MC control: states

(b) Comprehensive MC control: states

(c) Conventional MC control: signals

(d) Comprehensive MC control: signals

Fig. 2: Performance comparison of conventional (left) and Comprehensive (right) control schemes.

Note that the disturbance estimates ($\hat{d}_o$, $\hat{d}_1$ and $\hat{d}_2$) provided by the observers (4) and (5) are included in the equations (6). Eight equations (6) are solved together in the following way. The current references ($i_o^{*\alpha}$, $i_o^{*\beta}$) come from the load side (e.g. motor) control and are assumed known. Then ($v_o^{*\alpha}$, $v_o^{*\beta}$) can be determined from the two *Output* equations. This defines the right-hand side of the first *Extra* equation.

Next, state variables ($i_s^{*\alpha}$, $i_s^{*\beta}$), ($v_i^{*\alpha}$, $v_i^{*\beta}$) are expressed from the four *Input* equations in terms of the MC input ($i_i^{*\alpha}$, $i_i^{*\beta}$), known supply voltage ($v_s^{*\alpha}$, $v_s^{*\beta}$) and known disturbance estimates. Substitution into the two *Extra* equations allows one to find ($i_i^{*\alpha}$, $i_i^{*\beta}$). Other unknowns can be then found by back substitution.

Dynamic control

Dynamic control utilises state estimate feedback to regulate the state observer about the previously calculated sinusoidal steady state. The control laws for the input and output sides are given by, respectively:

$$i_i = i_i^* - K_1(\hat{i}_s - i_s^*) - K_2(\hat{v}_i - v_i^*); \qquad v_o = v_o^* - K_o(\hat{i}_o - i_o^*); \qquad \text{for} \quad \alpha,\beta \tag{7}$$

The control inputs i_i and v_o are determined from (7) independent of each other, and may contradict to the requirement of the instantaneous real power balance across the MC switches. This is resolved by "Control centre" shown in Fig.1b, as follows.

The supply side RLC filter, due to its resonant nature, requires an accurate and "aggressive" control. Hence the control gains K_1 and K_2 are designed to achieve "fast-acting" control poles. When defining the SVM switching pattern, the value of i_i determined from (7) is given preference to v_o. The v_o value found from (7) is projected onto the power balance constraint, and the constrained v_o^{con} nearest to v_o is determined and applied. Hence the applied values i_i and v_o^{con} are perfectly matched by the power balance.

Consequently, in transient, the load-side voltage v_o is driven by the instantaneous power balance with i_i, but its trend is to match the load-side current i_o with i_o^*. When approaching steady state, the load-side tracking is error-free, due to the use of the disturbance observer. In fact, steady state errors are eliminated on both sides due to inclusion of the disturbance estimates in the steady state reference calculations (6).

Comparison of Comprehensive to the conventional control of MC

To validate the proposed solution, a detailed simulation of an MC-based variable speed drive was set up in the Matlab/Simulink environment. The input side filter included $R_f = 2.5\Omega$; $L_f = 2.5$mH; $C_f = 14.2\mu$F. The input source was $V_s = 207V$(rms, line-to-line) at frequency 50Hz. The load side model represents an induction motor with $\sigma L_s = L_o = 52.3$mH; $R_s = R_o = 5\Omega$; and back-emf representing energy conversion from electromagnetic into mechanical.

Fig.2 compares performance of the conventional and the proposed control schemes under the following scenario: initially the load-side current reference is 3A; at time 0.05s this reference drops to 1.5A.

Figs.2a shows the state variables: $i_{s\alpha}$, $i_{s\beta}$, $v_{c\alpha}$, $v_{c\beta}$ for the MC input side and $i_{o\alpha}$, $i_{o\beta}$ for the MC output side under conventional control. The output-side states $i_{o\alpha}$, $i_{o\beta}$ are controlled by PI current control, and the input states are driven by the requirement of unity power factor. Fig.2b shows the same variables for the proposed control. The supply-side states $i_{s\alpha}$, $i_{s\beta}$ are controlled by state feedback current control, and the output-side states are driven to their steady-state references by integral action of the observers.

Fig.2c and Fig.2d compare the important MC input and output signals for the two control schemes. These signals include: the supply-side currents $i_s^{(abc)}$ plotted next to the scaled supply voltages $v_s^{(abc)}$ to illustrate the unity power factor; switched input-side current waveform $i_i^{(a)}$ and its low-frequency average; switched output-side voltage waveform $v_o^{(a)}$ and its low-frequency average; and the load-side currents $i_o^{(abc)}$ plotted next to their references to illustrate the reference tracking.

It can be observed from Fig.2 that, under the conventional control scheme, the change of the load-side current reference is accompanied by a resonant trace in the supply-side current. Additionally, even under steady state, the resonant component can be still observed in the supply-side current.

Both effects completely disappear when the proposed Comprehensive control scheme is applied. Under Comprehensive control, high-quality reference tracking and fast dynamic performance at the load side are achieved simultaneously with unity power factor and resonance suppression at the supply side.

Application of MC with Comprehensive control to on-board electric drives

Fig.3 illustrates performance of the proposed control under a simulated scenario of electric drive application. An additional problem that needed to be addressed in this case is power factor optimisation. The supply-side power factor has a complex and nonlinear dependence on the operating conditions [12]. Unity power factor cannot be always achieved [13].

The proposed control algorithm was modified so as to optimise power factor under every operating condition. Namely, if the power balance and the unity power factor requirements (labelled as *Extra* conditions in expressions (6)) are compatible, then unity power factor is achieved. Otherwise, the power balance condition is given preference, and power factor is made as close to unity as possible. This is achieved by implementing the following logic.

- The output side current control provides the reference vector $\bar{i}_o^*$. By solving the *Output* conditions in expressions (6), the $\bar{v}_o^*$ can be found. From that the output power requirement $P_o^* = v_o^{*\alpha} i_o^{*\alpha} + v_o^{*\beta} i_o^{*\beta}$ is determined;
- Two *Extra* conditions in expressions (6) conditions (power balance $P_i^* = P_o^*$ and the vector alignment $\bar{i}_s || \bar{v}_c$), are used simultaneously to determine the references vectors $\bar{i}_i^*$, $\bar{i}_s^*$ and $\bar{v}_c^*$;
- It is known from the literature [14] that the voltage transfer ratio for the MC, for a given input power factor, is limited by

$$q = \frac{V_o}{V_c \cos\varphi_i} \leq \frac{\sqrt{3}}{2} \quad \text{from which} \quad V_o^{max} = \frac{\sqrt{3}}{2} V_i \cos\varphi_i \tag{8}$$

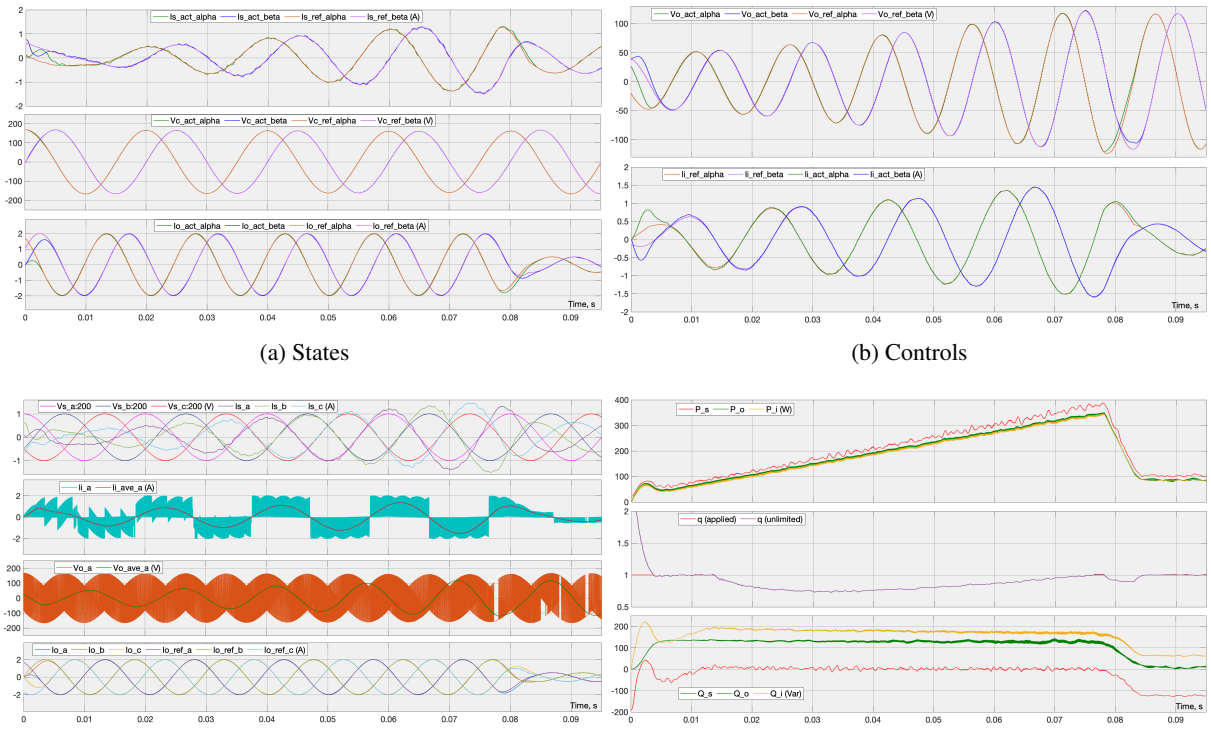

(a) States (b) Controls

(c) Signals (d) Powers and q

Fig. 3: Simulation plots for a MC-based variable speed drive operation.

On the other hand, from the input/output power balance, it follows that

$$\frac{V_o}{V_c \cos\varphi_i} = \frac{I_i}{I_o \cos\varphi_o} \quad \text{then} \quad I_i^{max} = \frac{\sqrt{3}}{2} I_o \cos\varphi_o \tag{9}$$

While condition (8) is more common in the literature, condition (9) is easier to check. The $\bar{i}_i^*$ magnitude is then compared to I_i^{max}. If $|\bar{i}_i^*| \leq I_i^{max}$ then the two *Extra* conditions are compatible, and unity power factor at the grid side can be achieved;

- Otherwise, the two *Extra* conditions are not compatible. Then the power balance condition is given preference, and power factor is made as close to unity as is possible for the given limitation I_i^{max} on the $\bar{i}_i^*$ magnitude. Then the second *Extra* condition in (6) is replaced by $(i_i^{*\alpha})^2 + (i_i^{\star\beta})^2 = I_i^{max}$, and the two updated *Extra* conditions are solved together. The updated solution for $\bar{i}_i^*$ and the corresponding solutions for the dependent vectors $\bar{i}_s^*$ and $\bar{v}_c^*$, are determined. The best possible (but not unity) grid-side power factor is automatically achieved.

- If, in the previous step, the solution for $\bar{i}_i^*$ cannot be found, then the demanded ($\bar{i}_o^*$, $\bar{v}_o^*$) combination cannot be produced under any grid-side power factor, and the MC enters an overmodulation mode.

Fig.3a shows the system state variables: $i_{s\alpha}$, $i_{s\beta}$, $v_{c\alpha}$, $v_{c\beta}$ for the MC input side and $i_{o\alpha}$, $i_{o\beta}$ for the MC output side. Fig.3b illustrates the control variables: $v_{o\alpha}$, $v_{o\beta}$ and $i_{i\alpha}$, $i_{i\beta}$. The actual look of the MC-generated signals (v_{oa} and i_{ia}) can be observed in Fig.3c, together with other phase signals of interest. Finally, Fig.3d illustrates the real powers (P_s at the supply, P_o at the MC output and P_i at the MC input), the normalised voltage transfer ratio $q = \frac{2}{\sqrt{3}} \frac{V_o}{V_c \cos\varphi_i}$ and the respective reactive powers (Q_s, Q_o and Q_i).

Initially, at the motor start and until $t = 0.0135$s, unity power factor at the MC supply side could not be achieved. As the motor speeds up and consumes more real power, the supply-side voltage and current come into alignment. This happens between $t = 0.0135$s and $t = 0.078$s. After reaching the rated speed

at $t = 0.078$s, the load torque reduces and, finally, settles at a new constant level corresponding to less than $1/3$ of the rated power at $t = 0.09$s. The supply-side power factor is 0.625 (leading).

An important observation from Fig.3 is that the proposed control scheme provides excellent reference tracking at the load side, operates in a stable and smooth manner, with no resonance excitation in the supply-side current and with maximum achievable supply-side power factor for every load-side condition. This makes Comprehensive control driving an MC-based electric drive a very attractive solution for electric transport applications.

Conclusion

This paper has explored a new Comprehensive control scheme for Matrix Converters intended for on-board electric drive applications. The paper has shown performance advantages of this scheme in comparison to the existing control methods. The paper has illustrated performance of Comprehensive control under simulated electric vehicle application scenario and has demonstrated excellent dynamics and reference tracking, smooth and stable operation, optimal handling of the power factor and effective resonance suppression.

References

[1] Khosravi M., Amirbande M., Khaburi D.A., Rivera M., Riveros J. et al: Review of Model Predictive Control strategies for Matrix Converters, 2019 IET Journal on Power Electronics, Vol 12 no 12, pp. 3021-3032

[2] Zhang J., Yang H., Wang T., Li L., Dorrell D.G. et al: Field-oriented control based on hysteresis band current controller for a permanent magnet synchronous motor driven by a direct matrix converter, 2018 IET Journal on Power Electronics, Vol 11 no 7, pp. 1277-1285

[3] Mirzaeva G., Seron M., Goodwin G.C.: Matrix Converters with input resonance suppression for mobile mining vehicles, 2020 IEEE IAS Annual Meeting, pp.1-5

[4] Lee K., Blaabjerg F.: Sensorless DTC-SVM for Induction Motor Driven by a Matrix Converter Using a Parameter Estimation Strategy, 2008 IEEE Transactions on Industrial Electronics, Vol 55 no2, pp.512-521

[5] Casadei D., Serra G., Tani A., Zarri L.: Matrix converter modulation strategies: a new general approach based on space-vector representation of the switch state, 2002 IEEE Transactions on Industrial Electronics, Vol 49 no 2, pp. 370-381

[6] Nguyen H.M., Lee H.H., Chun T.W.: Input power factor compensation algorithms using a new Direct-SVM method for matrix converter, 2011 IEEE Transactions on Industrial Electronics, Vol 58 no 1, pp. 232-243

[7] Lei J., Zhou B., Bian J., Wei J., Zhu Y. et al: Feedback control strategy to eliminate the input current harmonics of matrix converter under unbalanced input voltages, 2017 IEEE Transactions on Power Electronics, Vol 32 no 1, pp. 878-888

[8] Rivera M., Rodriguez J., Wheeler P.W., Rojas C.A., Wilson A. et al: Control of a matrix converter with imposed sinusoidal source currents, 2012 IEEE Transactions on Industrial Electronics, Vol 59 no 4, pp. 1939-1949

[9] Lei J., Feng S., Wheeler P., Zhou B., Zhao J.: Steady-state error suppression and simplified implementation of direct source current control for matrix converter With Model Predictive Control, 2020 IEEE Transactions on Power Electronics, Vol 35 no 3, pp. 3183-3194

[10] Rivera M., Amirbande M., Vahedi A., Tarisciotti L., Wheeler P.: Fixed frequency model predictive control with active damping for an indirect matrix converter, CHILECON 2017, pp.1-6

[11] Francis B.A., Wonham W.M.: The internal model principle of control theory, 1976 Automatica, no 12, pp. 457-465

[12] Nguyen H.N., Nguyen M.K., Duong T.D., Tran T.T., Lim Y.C. et al: A study on input power factor compensation capability of matrix converters, 2020 Electronics, Vol 9 no1, pp.82-99

[13] Mirzaeva G., Carter D., Seron M.: Grid-side power factor optimisation for Matrix Converters in mobile mining vehicle applications, 2021 IEEE IAS Annual Meeting, pp.1-6

[14] Huber L., Borojevic D.: Space vector modulated three-phase to three-phase matrix converter with input power factor correction, 1995 IEEE Transactions on Industry Applications, Vol 31 no 6, pp. 1234-1246